Anal. Bioanal. Electrochem., Vol. 16, No. 7, 2024, 683-699
https://www.doi.org/10.22034/abec.2024.714696

Analytical & Bioanalytical Electrochemistry

Full Paper

Inhibition of Copper Corrosion by Solanum Elaeagnifolium Extract in 0.5 M H_2SO_4 Solution

Abderrahmane Talfana, Issam Forsal,* and Sara Lahmady

Laboratory of Engineering and Applied Technologies, School of Technology, Beni Mellal, Morocco

*Corresponding Author, Tel.: +212661118208
E-Mail: forsalissam@yahoo.fr

Received: 29 January 2024 / Received in revised form: 29 June 2024 /
Accepted: 2 July 2024 / Published online: 31 July 2024

Abstract- Materials made with copper, find widespread use in various industries and several fields due to its important chemical and physical properties. However, these materials are susceptible to corrosion in harsh environments. This study explores the anti-corrosive properties of copper when exposed to solanum elaeagnifolium extract in 0.5 M H_2SO_4 solutions, employing electrochemical techniques such as electrochemical impedance spectroscopy and potentiodynamic polarization. The extract effectively protects by acting as a mixed-type inhibitor, as demonstrated by potentiodynamic polarization testing, with cathodic predominance. slowing down the cathodic and anodic reactions. An appropriate electrical analog circuit model was utilized to determine the electrochemical impedance characteristics. The analysis revealed that the inhibitor effectiveness is influenced by the inhibitor concentration, the temperature, and the exposure duration. This effectiveness achieved a maximum of 94% at a concentration of 2.5 g/L. The results obtained from electrochemical measurements are strongly supported by the examination of surface morphology. The addition of SE leads to a visibly smoother appearance of the copper, effectively suppressing corrosion of the copper sample. This observation implies the development of an SE–adsorption layer on the copper substrate.

Keywords- Copper; Sulphuric acid; Solanum elaeagnifolium extract; Potentiodynamic polarization; Electrochemical impedance spectroscopy

1. INTRODUCTION

Copper, a highly advantageous material employed by humans since antiquity, serves numerous applications owing to its exceptional characteristics such as high electrical conductivity, thermal conductivity, and commendable chemical resistance. It finds extensive utilization across various industrial sectors, encompassing electric power generation, heavy machinery manufacturing, defense applications, and construction projects [1]. The occurrence of corrosion or the development of oxide scales, resulting from exposure to harsh environmental conditions, can substantially diminish the thermal or electrical conductivity of copper. Consequently, the application of pickling solutions becomes imperative to eliminate corrosion byproducts and maintain the optimal performance of copper components [2]. Sulfuric acid serves as a commonly employed pickling solution for the removal of corrosion products from metal surfaces. Concurrently, it possesses the potential to induce corrosion on the metal substrate itself. To effectively mitigate the corrosion of the metal substrate, the addition of an inhibitor to the pickling solution becomes imperative [3].

Many inorganic and organic corrosion inhibitors raise environmental concerns. Consequently, the extensive application of these toxic substances is significantly constrained, particularly as public awareness of environmental preservation continues to advance [4]. Therefore, the development and utilization of corrosion inhibitors that are both environmentally friendly and efficient have become notably significant. These inhibitors preferentially accumulate at the metal-electrolyte interface via physical or chemical adsorption mechanisms. This accumulation creates a protective layer that hinders the diffusion of corrosive species towards the metal surface [5].

Recently, predominant emphasis has been directed towards the utilization of natural inhibitors, such as plant seeds [6], leaves, aqueous extracts from plants, peels, fruits, pectin, and lignin [7,8], as well as oil extracts [9,10] and alkaloid extracts from plants [7]. These substances are recognized as paramount and advantageous compounds due to their positive implications for both the environment and human well-being. Notably, they offer several advantages over chemical inhibitors, manifesting as nonpoisonous, cost-effective, environmentally benign, renewable, and readily accessible agents, thereby rendering them instrumental [11,12].

This research aims to examine the effective inhibition properties of SE extract on the corrosion of copper within a 0.5 M H_2SO_4 solution by using potentiodynamic polarization, and electrochemical impedance spectroscopy (EIS) methods. The study systematically explores the impact of SE extract concentration, temperature variations, and immersion time on the corrosion inhibition process. Additionally, Fourier-transform infrared spectroscopy (FTIR) is employed to discern and identify the specific functional groups present in the SE extract, contributing to a comprehensive understanding of its inhibitive characteristics.

2. MATERIALS AND METHODS

2.1. Solanum elaeagnifolium extract preparation methods

The preparation of solanum elaeagnifolium extract involved several steps. Firstly, the SE was obtained from a field in Beni mellal, Morocco. To prepare the powdered samples, leaves were thoroughly rinsed with distilled water on multiple occasions. Subsequently, they were desiccated for ten days at an ambient temperature of 298K. Finally, the leaves were pulverized into a powder using a crushing apparatus.

The dried SE was subjected to solvent extraction using ethanol. The mixture was magnetically stirred for 72 hours under ambient conditions (298K), then the solution was filtered by filter paper. Following this, the solvent was vaporized until a black liquid was obtained. The remaining ethanol was removed by drying the liquid in an oven, resulting in the formation of black powder that was used for the research.

2.2. Preparation of Working Electrode and Electrolyte Solution.

The experiment utilized a working electrode made of highly pure copper, which was sealed with epoxy resin for increased durability and stability. The surface area of the electrode was accurately measured to be 0.25 cm^2 using electrochemical techniques. Prior to each experiment, the electrode underwent meticulous preparation, including sequential polishing with emery paper of different grits (400, 600, 800, 1000, 1200, 1500, and 2000). To ensure a contaminant-free surface, the electrodes were subjected to a multi-step cleaning procedure. Initially, they were rinsed with deionized water to remove surface debris. Subsequently, thorough degreasing was achieved using acetone. This was followed by a final rinse with deionized water to eliminate any residual particles generated during the grinding process, such as sandpaper grit and copper shavings. Finally, the electrodes were dried using a stream of cold air.

The corrosion tests were initiated by immersing the prepared working electrode in a 0.5 M H_2SO_4 solution. This solution was prepared by mixing 98 wt% H_2SO_4 with ultrapure water. Various concentrations of SE ranging from 0.5 to 2.5 g/L were used in the experiments. Additionally, the 0.5 M H_2SO_4 solution was taken as the blank for comparison. It is important to note that the SE solution was prepared in advance and consistently used in each experiment.

2.3. Electrochemical measurements

A conventional three-electrode configuration was employed for the electrochemical measurements. This setup comprised a working electrode made of copper, a platinum foil counter electrode with a geometric area of 1 cm^2, and a saturated calomel electrode (SCE) as the reference electrode. An electrochemical workstation (Origa-Master) was used to conduct the experiments.

Prior to electrochemical testing, the working electrode was immersed in the test solution and subjected to an OCP scan for 1800 seconds to establish a stable potential. Subsequently, EIS was performed at the OCP using a 10 mV peak-to-peak AC perturbation and a frequency range of 100 kHz to 10 mHz. The acquired impedance data were then analyzed and fitted using dedicated EC-Lab software. Following EIS, PDP test was carried out, sweeping the potential from the OCP within a ±250 mV range at a scan rate of 2 mV/s. The resulting polarization curve data were directly analyzed using the electrochemical workstation software. To enhance data robustness and minimize potential errors, all measurements were performed in triplicate under identical experimental conditions.

2.4. FTIR analysis.

The FTIR analysis was performed using an FTIR spectrometer (Thermo Scientific Nicolet IS50 spectrophotometer) equipped with an attenuated total reflectance (ATR) sampling accessory. The SE sample was scanned over the range of 4000 cm^{-1} to 500 cm^{-1} with a resolution of 16 cm^{-1}.

2.5. Analysis of surface morphology

To investigate the surface morphology of the corroded and protected copper samples, Field-Emission Scanning Electron Microscopy (FE-SEM) analysis was performed at 298K. The copper specimens were prepared by abrading with a sequence of silicon carbide (SiC) sandpaper grits ranging from 400 to 2000, followed by thorough rinsing. Subsequently, the Cu blocks were immersed in a sulfuric acid solution for 24 hours. One set of samples was immersed in the bare acid solution, while another set was exposed to the acid solution containing 2.5 g/L of the selected inhibitor (SE).

3. RESULTS AND DISCUSSION

3.1. Analysis of potentiodynamic polarization curves

3.1.1. Open circuit potential measurements.

The evolution of the open circuit potential (OCP) primarily reflects the transformation of the electrode from an unstable to a stable state. Figure 1(a) showcases the OCP-time curves. When compared to a solution without SE, every E_{ocp} curve exhibited a noticeable shift towards the negative direction, and the existence of SE induces a corrosion electric displacement towards the cathode area, The observed behavior suggests that SE undergoes an adsorption process at the copper interface. Furthermore, the deviation of E_{ocp} values, being less than 85 mV, suggests that SE acts as a mixed-type inhibitor with cathodic predominance [13].

3.1.2. Polarization curves

The assessment of corrosion inhibition performance is conveniently conducted through potentiodynamic polarization measurements. Figure 1(b) presents the potentiodynamic polarization curves for Cu in a 0.5M H_2SO_4 solution at 298 K, encompassing various concentrations of SE.

EIS data reveals a significant decrease in corrosion current density (icorr) with increasing SE concentration, evident in both the cathodic and anodic polarization curves. This suggests the successful inhibition of both anodic copper dissolution and cathodic reduction reactions. Notably, the cathodic curves for different SE concentrations exhibit minimal deviation, implying that SE adsorption on the copper electrode surface does not significantly alter the underlying cathodic reaction mechanism. Interestingly, the presence of SE introduces a plateau region in the anodic curves at a potential range of -0.04 to -0.01 V (vs. SCE). This plateau likely originates from the formation of a dense adsorption film on the Cu/solution interface due to SE accumulation, potentially leading to a passivation effect that hinders anodic dissolution.

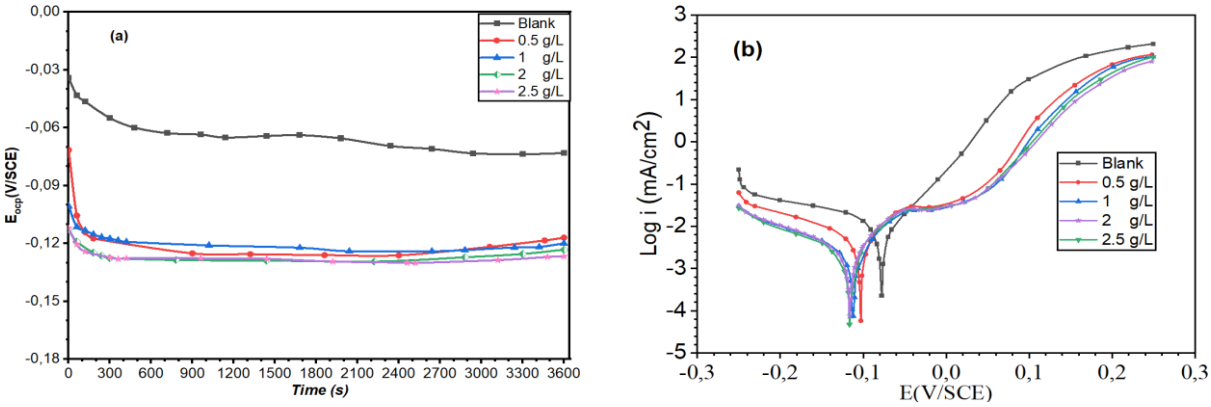

Figure 1. Presents the electrochemical response of an electrode immersed in 0.5 M H_2SO_4 solution containing varying SE concentrations at 298 K; (a) depicts the OCP diagrams, while (b) shows the PDP curves

The utilization of the extrapolation method within the Tafel region, a strongly polarized section of polarization curves, proves valuable in gaining insights into the changes observed in the cathodic and anodic behavior of copper. Through extrapolation, several parameters can be determined, including E_{corr} (self-corrosion potential), i_{corr} (corrosion current density), β_a (anode Tafel slope), and β_c (cathode Tafel slope), To determine η%, the following formula should be employed [14]:

$$\eta\% = \frac{i_{corr,o} - i_{corr}}{i_{corr,o}} \times 100 \qquad (1)$$

As presented in Table 1, the corrosion current (i_{corr}) in the absence of SE within the blank solution measures 10.83 μA.cm^{-2}. Upon introducing SE at a concentration of 2.5 g/L, the corrosion current density on the Cu electrode surface markedly decreases to 0.74 μA cm^{-2}, indicating a substantial corrosion inhibition efficiency of 93%. This compelling evidence strongly supports the high-quality anti-corrosive properties of SE. Furthermore, the corrosion potential in the absence of SE is recorded at −77.64 mV, while with the addition of SE, the corrosion potential ranges from −103 mV to −116 mV. Given that the voltage change remains below 85 mV, our findings classify SE as a mixed-type inhibitor with cathodic predominance [15].

Table 1. The parameters obtained from the PDP curves of a Cu electrode immersed in a 0.5 M H_2SO_4 solution at 298 K

C (g/L)	E_{corr} (mV/SCE)	I_{corr} (μA.cm^{-2})	βc (mV.dec^{-1})	βa (mV.dec^{-1})	Ƞ (%)
Blank	-77.641	10.83	157.70	93.50	-----
SE					
0.5	-103.202	1.88	43.4	38.51	83
1	-112.221	1.08	88.2	48.00	90
2	-115.742	0.96	40.4	26.70	91
2.5	-116.11	0.74	27.7	23.70	93

3.2. EIS for characterizing material properties

EIS experiment provides a rapid means to acquire information regarding the dynamics and interface structure on the surface of the WE. As a result, it is widely employed in the field of metal protection. Figure 2 illustrates the Nyquist diagram for copper at 298 k under varying concentrations of SE.

In Figure 2, the unaltered EIS curve displays a high-frequency capacitive semicircle along with a low-frequency oblique line, known as the Warburg impedance. The presence of this oblique line at low frequencies indicates that H_2SO_4 has initiated corrosion on the copper surface. Consequently, the corrosion byproducts either dissolve into the surrounding solution or O_2 diffuses towards the surface [16].

However, when SE is introduced, the size of the capacitive semicircle grows, and this increase continues with higher concentrations of SE. Simultaneously, the Warburg impedance

disappears entirely. This observation suggests that SE forms a protective barrier film, reducing copper corrosion and preventing the diffusion processes involving corrosion products and oxygen.

Regrettably, the measured capacitive semicircle consistently deviates from the expected standard, a phenomenon referred to as frequency dispersion [17]. While the exact cause of this phenomenon remains unclear, it is evident that it is linked to factors such as the unevenness of the Cu surface, the presence of adsorption layers, and the conductivity of the solution [18].

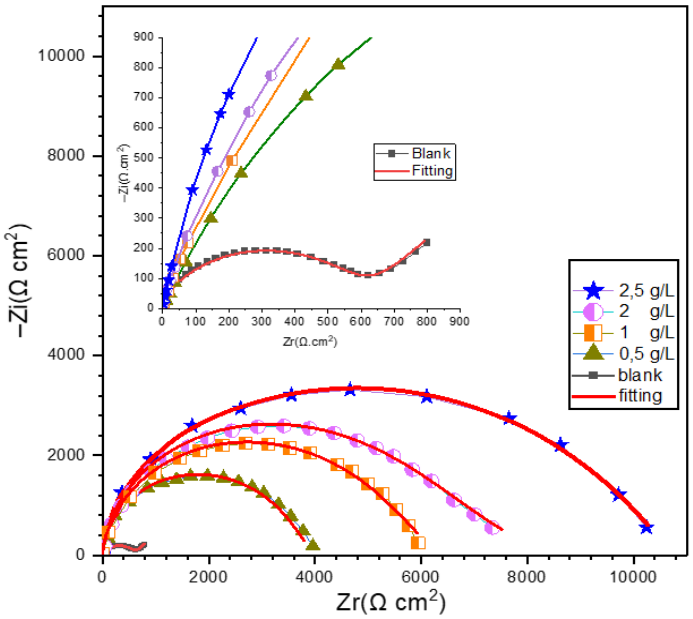

Figure 2. shows Nyquist plots for a copper electrode immersed in 0.5 M H_2SO_4 with different SE concentrations, all measured at 298 K

The equivalent circuit diagrams depicted in Figure 3(a) and (b) serve the purpose of fitting the EIS results, with and without Warburg impedance, respectively. The impedance spectra data obtained from the fitting process are detailed in Table 2. R_f represents the film resistance, R_{ct} denotes the charge transfer resistance, and the sum of R_f and R_{ct}, denoted as R_p, represents the polarization resistance, Additionally, W is the Warburg impedance Finally, the constant phase angle elements, CPE_{dl} and CPE_f, are introduced to account for the non-idealities of the double layer capacitance (C_{dl}) and the film capacitance (C_f), respectively.

The characterization of CPE impedance is articulated as follows [19-21]:

$$Z_{CPE} = \frac{1}{y_0(j\omega)^n} \qquad (2)$$

CPE is denoted by y_0, where j represents the imaginary unit and ω signifies the angular frequency. The deviation parameter (n) reflects the degree of heterogeneity on the electrode

surface. Additionally, the capacitance values for the double-layer (C_{dl}) and the coating layer (C_f) can be determined using Equations (3) and (4), respectively [22]:

$$C_{dl} = y_0^{1/n}\left(\frac{1}{R_s} + \frac{1}{R_{ct}}\right)^{(n-1)/n} \quad (3)$$

$$C_f = y_0(2\pi f_{max})^{n-1} \quad (4)$$

The capacitance values of C_{dl} and film (C_f) are presented in Table 2. A gradual decrease in both C_{dl} and C_f is observed with increasing SE concentration. This trend can be further analyzed using the equations provided in formulas (5) and (6) [23]:

$$C_f = \frac{F^2 S}{4RT} \quad (5)$$

$$C_{dl} = \frac{\varepsilon^0 \varepsilon}{d} S \quad (6)$$

In the provided formula, F denotes the Faraday constant, while ε^0 and ε respectively signify the air dielectric constant and the local dielectric constant of the double layer. S represents the exposed area of the copper electrode in the H_2SO_4 environment, and d corresponds to the thickness of the C_{dl}. The reduction in both C_{dl} and the C_f indicates the replacement of H_2O molecules on the copper surface by SE molecules. Consequently, the values of C_f and C_{dl} exhibit an inverse relationship with the anti-corrosion efficiency (η). To quantify η%, the following equation can be employed [24]:

$$\eta\% = \frac{R_P - R_{P,0}}{R_P} \times 100 \quad (7)$$

The R_p and $R_{p,0}$ represent the polarization resistance in the presence and absence of SE. As shown in Table 2, the values of C_f and C_{dl} exhibit a consistent decrease with the emergence of SE, while both R_f and R_{ct} noticeably increase [25].

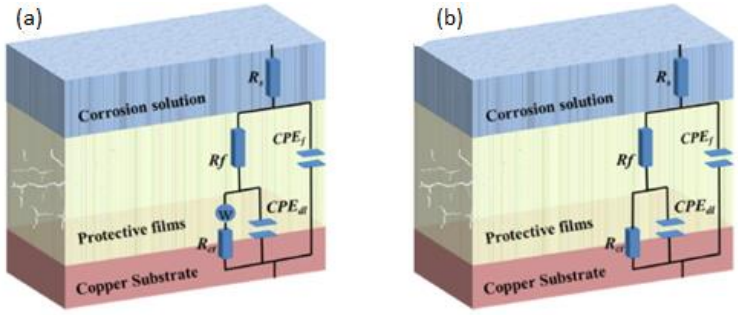

Figure 3. Presents two equivalent circuit diagrams for analyzing EIS data: (a) depicts the circuit used for fitting data with a Warburg element, whereas (b) illustrates the circuit for data without a Warburg element.

Additionally, the inhibition efficiency shows a continuous rise with increasing concentration, indicating the adsorption of more SE molecules on the electrode. This phenomenon contributes to a negative catalytic effect on copper corrosion. It's noteworthy to highlight that A high degree of consistency is observed between the inhibition efficiencies measured using EIS and PDP techniques.

Table 2. EIS parameters were utilized to evaluate the effectiveness of corrosion inhibitors for protecting Cu electrodes immersed in 0.5 M H_2SO_4 at 298 K

C (g/L)	R_f ($\Omega.cm^2$)	R_{ct} ($\Omega.cm^2$)	R_p ($\Omega.cm^2$)	C_f ($\mu f.cm^{-2}$)	n1	C_{dl} ($\mu f.cm^{-2}$)	n2	W ($\times 10^2\ \Omega.cm^2\ s^{1/2}$)	Ŋ (%)
Blank SO	12	607	619	51.5	0.84	87.72	0.66	1.72	---
0.5	13.03	4040	4053.03	23.02	0.996	28.55	0.41	------	85
1	6.23	6 148	6154.23	33.37	1	19.8	0.47	------	90
2	27.03	7885	7912.03	17.73	1	20.88	0.36	------	92
2,5	61.76	10500	10561.76	28.29	0.99	17.04	0.48	------	94

3.3. Effect of temperature on inhibition

Examining the corrosion mechanism broadly, temperature plays a crucial role. This is attributed to its influence on metal-electrolyte interaction, making it an important factor in the research [26,27]. This enables us to assess how SE is adsorbed onto the copper surface and determine the stability of SE with increasing temperature.

3.3.1. Polarization curves

Figure 4 illustrates the polarization curves acquired for Cu in a 0.5M H_2SO_4 solution, both in the absence and presence of 2.5 g/L SE, at varying temperatures. The pertinent parameters are detailed in Table 3. Irrespective of the presence of 2.5 g/L SE in the solution, the curves shift towards higher current densities as the temperature rises. Notably, each polarization curve remains nearly parallel to the others, indicating that the corrosion mechanism is unaffected by temperature variations. The i_{corr} values increase proportionally with temperature, signifying accelerated corrosion of Cu with rising temperature. Upon introducing 2.5 g/L SE at each temperature, the i_{corr} decreases compared to the SE-free solution, underscoring the substantial corrosion inhibition effect of SE. Additionally, as the solution temperature increases, the η values decrease due to the weakening of the adsorbed SE film on the Cu substrate. Remarkably, even at 328 K, SE demonstrates outstanding inhibition performance, suppressing copper corrosion by 84%.

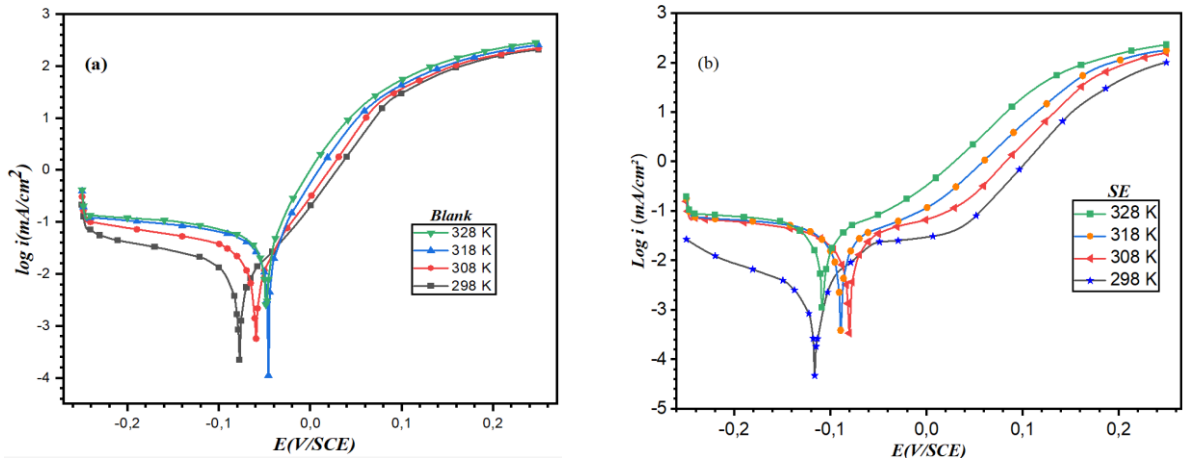

Figure 4. Potentiodynamic polarization curves for copper in 0.5M H_2SO_4 without (a) and with 2.5 g/L of SE (b) at different temperatures

Table 3. Electrochemical parameters are measured for cu electrodes in a 0.5 M H_2SO_4 solution at various temperatures (298 K to 328 K), with and without the presence of different SE concentrations

T (K)	C (g/L)	E_{corr} (mV/SCE)	I_{corr} (µA.cm^{-2})	βc(mV.dec^{-1})	βa (mV.dec^{-1})	ŋ (%)
298	0	-77.641	10.83	157.70	93.50	------
	2.5	-116.11	0.74	27.7	23.70	93
308	0	-59.38	25.82	47.8	107	------
	2.5	-80.95	2.61	27.1	25.2	90
318	0	-46.83	37.23	32.6	180	------
	2.5	-90	5.08	35	37.9	86
328	0	-47	44.95	36.1	238	------
	2.5	-109	7.17	38.4	46	84

3.3.2. EIS analysis.

To evaluate the inhibitor film's persistence, additional electrochemical experiments were performed at varying temperature conditions. Figure 5 presents Nyquist plots that illustrate the impedance behavior of a Cu electrode immersed in a 0.5 M H_2SO_4 solution at different temperatures. The plots depict the response with and without the presence of 2.5 g/L SE. Notably, the diameter of the capacitive loop in both the blank and inhibited solutions decreases as the temperature rises, suggesting an accelerated corrosion rate of copper with increasing temperature. Furthermore, the impedance experiences a significant increase in the presence of SE compared to inhibitor-free solutions at each temperature.

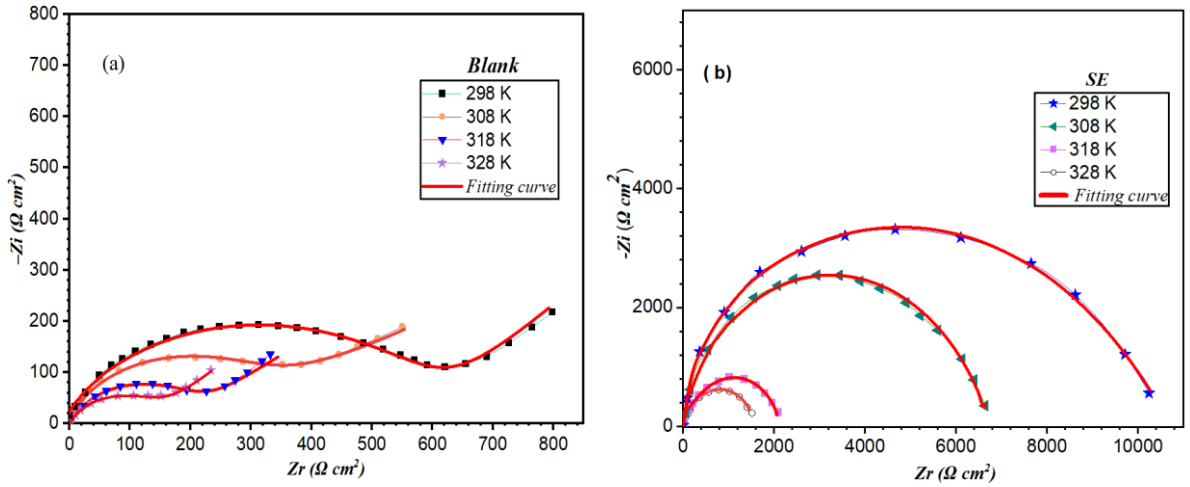

Figure 5. Nyquist curves for cu in 0.5 M H_2SO_4 solution in the absence and presence of 2.5 g/L SE at different temperatures

Analysis of the fitted EIS data (Table 4) revealed a temperature dependence on the electrochemical parameters. Increasing temperature resulted in higher capacitance values (C_f and C_{dl}) and lower resistance (R_f), charge transfer resistance (R_{ct}), and inhibition efficiency (η). This trend can be attributed to enhanced molecular motion at elevated temperatures, hindering the formation of a stable SE adsorption layer and promoting charge transfer during the corrosion process [28]. However, compared to uninhibited solutions at each temperature, the presence of SE consistently elevated Rf and R_{ct} values while lowering Cf and C_{dl} values. Notably, the achieved inhibition efficiency (η) remained high across the temperature range. These observations suggest that SE effectively shields the copper surface at all tested temperatures, despite the accelerating effect of temperature on corrosion. This implies the formation of an adsorption film on the copper substrate by SE, even under elevated thermal conditions.

Table 4. The parameters extracted from equivalent circuit fitting of EIS data were used to characterize the electrochemical behavior of cu electrodes in 0.5 M H_2SO_4 solution

T (K)	C (g/L)	R_f (Ω cm²)	R_{ct} (Ω cm²)	R_p (Ω cm²)	C_f (µf cm²)	n1	C_{dl} (µf cm²)	n2	W ($\times10^2\Omega cm^2 s^{1/2}$)	η(%)
298	0	12	607	619	51.5	0.84	87.72	0.66	1.72	------
	2.5	61.76	10500	10561.76	28.29	0.99	17.04	0.48	------	94
308	0	7	380.73	387.73	64.3	0.92	95.08	0.87	1.43	------
	2.5	20.8	6617	6637.8	37.66	1	18.73	0.6	------	94
318	0	3	214.25	217.25	82.05	0.97	106.56	0.64	1.55	------
	2.5	32.527	2312	2344.52	102	1	27.55	0.54	------	91
328	0	1.1	151.7	152.8	86.9	0.72	121.51	0.98	1.38	------
	2.5	8.79	1592	1600.79	171	0.81	56.76	0.8	------	91

3.4. Immersion time effect on corrosion inhibition

Examining the protective performance of SE for copper in aggressive environments also requires considering the element of time as a crucial factor. therefore, the EIS data for Cu immersed in an acidic solution, both with and without 2.5g/L SE, were measured at various time intervals (1-24 h), as illustrated in Figure 6. As the immersion time prolongs, the blank capacitive semicircle consistently diminishes, signifying the progressive corrosion of copper. when introducing 2.5 g/L SE, the capacitive semicircle exhibits a decrease within the initial 2 h and remains in decrease from 2 to 24 h. After 24 h, despite the decrease in the capacitive half-circle, it remains substantially huge than the blank one.

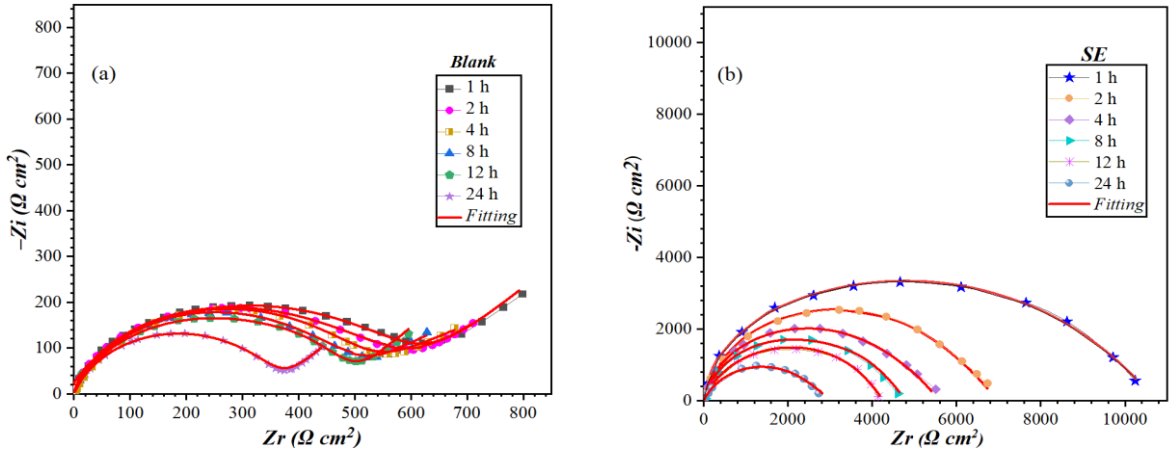

Figure 6. Curves Nyquist plots in: a) 0.5 M H_2SO_4 and b) 0.5 M H_2SO_4 + 2.5 g/L of SE extract, with different times of immersion, at 298 K

Table 5. Cu electrochemical parameters in 0.5 M H_2SO_4 and 0.5 M H_2SO_4 + 2.5 g/L of SE extract, with different times of immersion, at 298K

t (h)	C (g/L)	Rf (Ω cm²)	R_{ct} (Ω cm²)	R_p (Ω cm²)	C_f (μf cm^{-2})	n1	C_{dl} (μf cm^{-2})	n2	W ($\times10^2\Omega cm^2 s^{1/2}$)	η(%)
1	0	12	607	619	51.5	0.84	87.72	0.66	1.72	------
	2.5	61.76	10500	10561.76	28.29	0.99	17.04	0.48	------	94
2	0	11	559	570	54	0.97	98	0.95	1.63	------
	2.5	49	6851	6900	29	0.9	32	O.4	------	92
4	0	8	527	535	62	0.99	114	0.89	1.54	------
	2.5	50	5650	5700	35	1	63	0.67	------	91
8	0	5	495	500	93	0.89	120	0.45	1.51	------
	2.5	32	4668	4700	39	0.98	68	0.76	------	89
12	0	1	469	470	101	0.95	138	0.66	1.48	------
	2.5	42	4162	4204	41	1	79.3	0.73	------	89
24	0	0.6	369.4	360	122	0.93	223	0.8	1.3	------
	2.5	25.36	2903	2928.36	54	0.999	91	0.6	------	88

Table 5 demonstrates a significant enhancement in both resistance (Rf) and charge transfer resistance (Rct) for samples immersed with 2.5 g/L SE compared to the blank solution after 24 hours. Conversely, capacitance values (C_f and C_{dl}) for the SE-treated samples were noticeably lower than those of the blank. Notably, the achieved inhibition efficiency (η) for copper with 2.5 g/L SE reached 88% after 24 hours. This suggests that SE molecules effectively form a protective film on the copper surface, hindering corrosion processes during the immersion period.

3.5. FTIR analysis.

Figure 7 presents the FTIR spectrum of SE. The spectrum reveals the presence of several functional groups potentially responsible for its promising corrosion inhibition performance. Characteristic absorption bands were observed at various wavenumbers: 3269 cm^{-1} (indicative of O-H stretching) [29], 2925 cm^{-1} (attributed to C-H stretching) [30], 1605 cm^{-1} (potentially corresponding to C=C or C=N) [31], and 1373.5 cm^{-1} (likely due to O-H bending). Additionally, bands at 1247 cm^{-1} suggest the presence of aromatic rings, while peaks below 1000 cm^{-1} attributed to C-H stretching of aromatic and aliphatic groups. These findings suggest that SE possesses a diverse range of functional groups, including hydroxyl, carbonyl, C-C/nitrogen double bonds, and aromatic moieties. Notably, such functional groups are often associated with effective adsorption onto metal surfaces, potentially explaining the observed corrosion inhibition properties of SE [32–34].

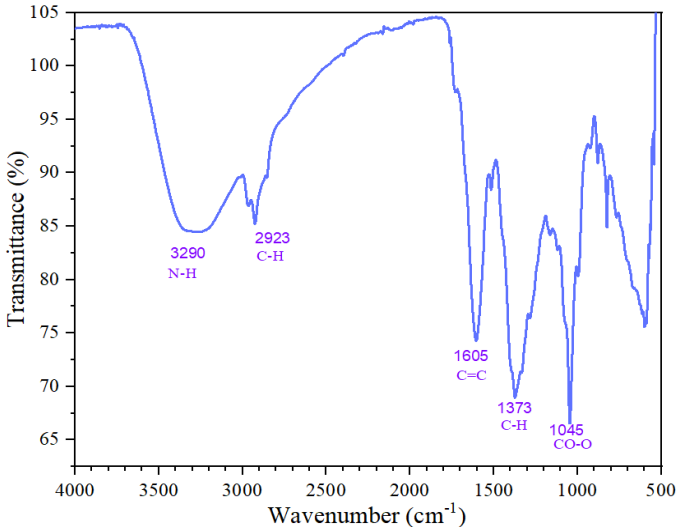

Figure 7. FTIR spectrum of pure SE

3.6. SEM surface morphology analysis

At a temperature of 298 K, we examined the copper morphology using scanning electron microscopy in both a 0.5M sulfuric acid solution with and without a corrosion inhibitor. The

copper sample had dimensions of 5 mm×5 mm×2 mm, and the results are depicted in Figure 8. Figure 8(a) displays an untreated, recently polished copper block characterized by a smooth, flat surface and minor scratches resulting from the polishing process. In Figure 8(b), the image portrays a copper specimen immersed in a 0.5 M H_2SO_4 solution for 24 h at 298 K, revealing a rough and uneven surface in the absence of a corrosion inhibitor. This signifies noticeable corrosion of the copper block in the uninhibited solution. Figure 8(c) presents scanning electron micrographs of copper blocks immersed in a 0.5 M sulfuric acid solution with a corrosion inhibitor (SE). The addition of the corrosion inhibitor leads to a visibly smoother appearance of the copper, effectively suppressing the corrosion of the copper sample. This observation suggests the formation of an SE–adsorption film on the Cu substrate.

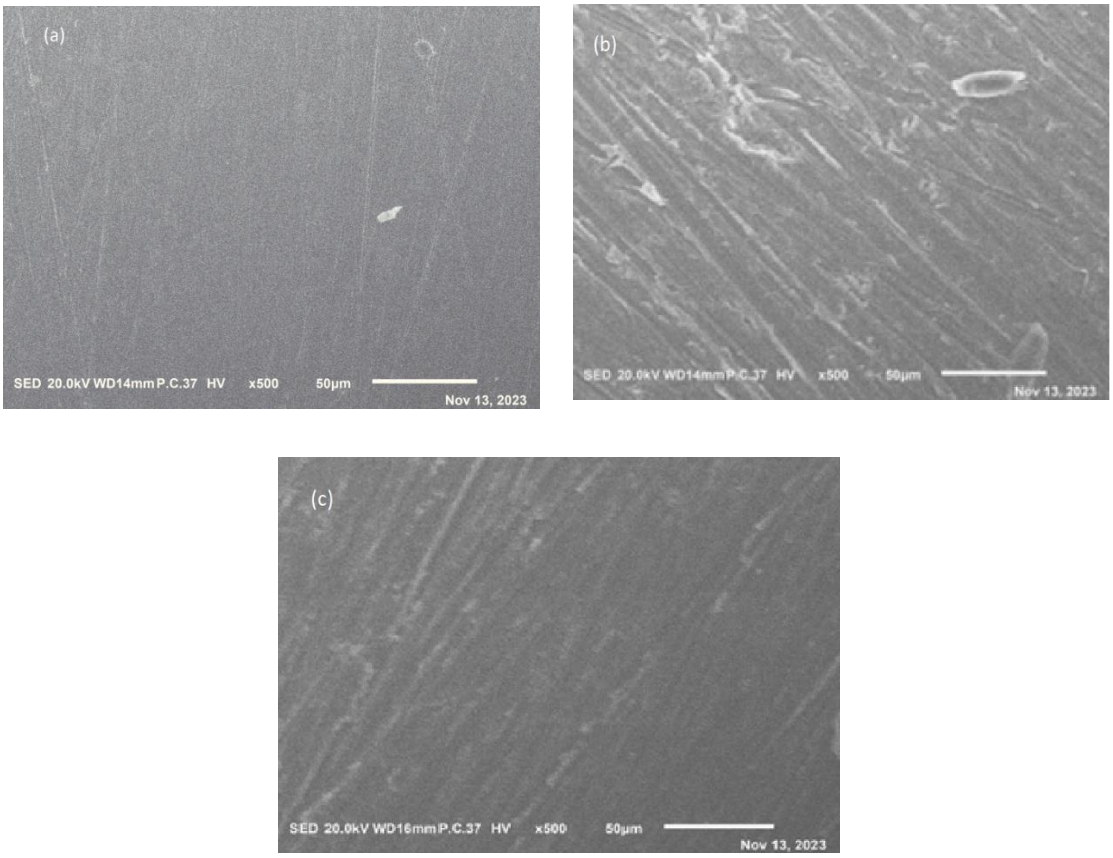

Figure 8. SEM image at the surface of Cu immersed in 0.5 M H_2SO_4 solutions with 0 and 2.5g/L SE for 24 h at 298 K

4. CONCLUSION

The present work investigated the corrosion inhibition performance of a novel inhibitor, designated as SE, on copper in a 0.5 M sulfuric acid medium. A combined approach utilizing electrochemical measurements and surface characterization techniques was employed. The results demonstrated that SE possesses promising inhibitory potential, achieving a maximum efficiency of 94% at 2.5 g/L and room temperature. The inhibitor's functional groups likely

facilitate adsorption onto the copper surface, as evidenced by the achieved efficiency. Tafel polarization analysis suggests a mixed-type inhibition mechanism with a dominant effect on the cathodic reaction. Furthermore, SE exhibited remarkable thermal stability, maintaining good inhibition efficacy at elevated temperatures. Finally, SEM analysis corroborated the formation of a protective layer on the copper surface by SE, reinforcing its potential as a corrosion inhibitor for Cu in acidic environments.

Abbreviations

βa: Anodic Tafel slope
βc: Cathodic Tafel slope
C: Capacitor
CE: Counter electrode
$C_{\mathbf{R}}$: Corrosion rate
Cu: Copper
CPE: Constant phase element
E: Potential
E_{corr}: Corrosion potential
EIS: Electrochemical impedance spectroscopy
H_2SO_4: Sulphuric acid
Icorr: Corrosion current density
η %: Inhibition efficiency
OCP: Open circuit potential
PDP: Potentiodynamic polarization
Q_{dl}: Double layer charge
RE: Reference electrode
R_{ct}: Charge transfer resistance
SC: Saturated calomel
SR: Scan rate
WE: Working electrode
SE: Solanum elaeagnifolium
SEM: Scanning electrode microscope

Declarations of interest

The authors declare no conflict of interest in this reported work.

REFERENCES

[1] M.A. Deyab, J. Ind. Eng. Chem. 22 (2015) 384.
[2] B. Tan, S. Zhang, W. Li, X. Zuo, Y. Qiang, L. Xu, J. Hao, and S. Chen, J. Ind. Eng. Chem. 77 (2019) 449.
[3] B. Tan, S. Zhang, J. He, W. Li, Y. Qiang, Q. Wang, C. Xu, and S. Chen, J. Mol. Liq. 321 (2021) 114464.
[4] Y. Qiang, S. Zhang, L. Guo, X. Zheng, B. Xiang, and S. Chen, Corros, Sci. 119 (2017) 68.

[5] D. Fu, B. Tan, L. Lu, X. Qin, S. Chen, and W. He, J. Chen, Int. J. Electrochem. Sci. 13 (2018) 8561.
[6] A.H. Mostafatabar, G. Bahlakeh, B. Ramezanzadeh, A. Dehghani, and M. Ramezanzadeh, J. Mol. Liq. 331 (2021) 115764.
[7] B.E.A. Rani, and B.B.J. Basu, Int. J. Corr. 2012 (2012) 380217.
[8] M. Abdallah, H.M. Altass, B. Al Jahdaly, and M. Salem, Green Chem. Lett. Rev. 11 (2018) 189.
[9] S. Cherrad, A.A, Alrashdi, H.S. Lee, Y. Elaoufir, H. Lgaz, B. Satrani, M. Ghanmi, E. Aouane, and A. Chaouch, Arabian. J. Chem. 15 (2022) 103849.
[10] K.M. Oladipupo Kareem, A.A. Edathil, K. Rambabu, G. Bharath, F. Banat, G.S. Nirmala, and K. Sathiyanarayanan, Chem. Eng. Commun. 208 (2021) 801.
[11] B.R. Fazal, T. Becker, B. Kinsella, and K. Lepkova, Materials Degradation 6 (2022) 1.
[12] A. Kouache, A. Khelifa, H. Boutoumi, S. Moulay, A. Feghoul, B. Idir, and S. Aoudj. Adhesion. Sci. Technol. 36 (2022) 988.
[13] Y. Qiang, S. Zhang, H. Zhao, B. Tan, and L. Wang, Corrosion. Science. 161 (2019) 108193.
[14] Y. Qiang, S. Zhang, and L. Wang, Applied Surface Sci. 492 (2019) 228.
[15] B. Tan, S. Zhang, H. Liu, Y. Guo, Y. Qiang, W. Li, L. Guo, C. Xu, and S. Chen, Colloid Interface Sci. 538 (2019) 519.
[16] B. Tan, S. Zhang, Y. Qiang, W. Li, H. Li, L. Feng, L. Guo, C. Xu, S. Chen, and G. Zhang, J. Mol. Liq. 298 (2020) 111975.
[17] X. Ma, J. Wang, S. Yu, X. Chen, J. Li, H. Zhu, and Z. Hu, J. Mol. Liq. 315 (2020) 113711.
[18] H. Li, S. Zhang, B. Tan, Y. Qiang, W. Li, S. Chen, and L. Guo, J. Mol. Liq. 305 (2020) 112789.
[19] K. Haruna, I.B. Obot, N.K. Ankah, A.A. Sorour, and T.A. Saleh, J. Mol. Liq. 264 (2018) 515.
[20] F. El-Hajjaji, M. Messali, A. Aljuhani, M.R. Aouad, B. Hammouti, M.E. Belghiti, D.S. Chauhan, and M.A. Quraishi, J. Mol. Liq. 249 (2018) 997.
[21] H. Gerengi, M.M. Solomon, S. Ozturk, A. Yildirim, G. Gece, and E. Kaya, Mater. Sci. Eng. C 93 (2018) 539.
[22] Y. Qiang, H. Li, and X. Lan, Mater. Sci. Technol. 52 (2020) 63.
[23] B. Tan, S. Zhang, Y. Qiang, L. Guo, L. Feng, C. Liao, Y. Xu, and S. Chen, Colloid Interface Sci. 526 (2018) 268.
[24] S. Lahmady, O. Anor, I. Forsal, B. Mernari, H. Hanin, K. Benbouya, and A. Talfana, Portugaliae Electrochim. Acta 41 (2023) 135.
[25] G. Quartarone, M. Battilana, L. Bonaldo, and T. Tortato, Corr. Sci. 50 (2008) 3467.
[26] G. Mu, and Li. X, Colloid Interface Sci. 289 (2005) 184.
[27] M.A. Deyab, Solid State Electrochem. 13 (2009) 1737.

[28] H. Tian, W. Li, and B. Hou, Corr. Sci. 53 (2011) 3435.
[29] O. Anor, S. Lahmady, I. Forsal, H.Hanine, H. Ourradi, and A. Elharami, Biointerface Research in Applied Chem. 13 (2023) 271.
[30] M.K. Oladipupo, A.A. Edathil, K. Rambabu, G. Bharath, F. Banat, G.S. Nirmala, and K. Sathiyanarayanan, Chem. Eng. Commun. 208 (2021) 801.
[31] N.Y. Abu-Thabit, A.A Judeh, A.S. Hakeem, A. Ul-Hamid, Y. Umar, and A. Ahmad, Int. J. Biological Macromolecules 155 (2020) 730.
[32] Z. Sanaei,M. Ramezanzadeh, G. Bahlakeh, and B. Ramezanzadeh, J. Ind. Eng. Chem. 69 (2019) 18.
[33] Y. Qiang, S. Zhang, B. Tan, and S. Chen, Corr. Sci. 133 (2018) 6.
[34] A. Habibiyan, B. Ramezanzadeh, M. Mahdavian, and M. Kasaeian, J. Mol. Liq. 298 (2020) 111974.